Acta Materialia 147 (2018) 16–23

Contents lists available at ScienceDirect

Acta Materialia

journal homepage: www.elsevier.com/locate/actamat

Thermodynamic mixing energy and heterogeneous diffusion uncover the mechanisms of radiation damage reduction in single-phase Ni-Fe alloys

Miaomiao Jin, Penghui Cao*, Michael P. Short

Department of Nuclear Science and Engineering, Massachusetts Institute of Technology, Cambridge, MA 02139, USA

ARTICLE INFO

Article history:
Received 25 September 2017
Received in revised form
18 December 2017
Accepted 19 December 2017
Available online 6 February 2018

Keywords:
Atomistic simulation
Ion irradiation
Damage reduction mechanisms
Heterogeneous diffusion
Single-phase alloys

ABSTRACT

Understanding and predicting radiation damage is of central importance to develop radiation-tolerant structural materials for current and next-generation nuclear systems. Single-phase solid solution alloys constitute attractive choices due to their promising mechanical properties and radiation tolerance. Here, by examining radiation-induced defect production and evolution in single-phase Ni-Fe alloys, we show that radiation damage resistance directly correlates with thermodynamic mixing energy and heterogeneity of defect diffusion. We found that radiation damage in materials decreases linearly with lowering mixing energy, and the relationship holds true for all studied Ni-Fe compositions. The damage reduction with varying composition is further ascribed to the increasing heterogeneity of point defect migration across a complex potential energy landscape that enhances defect recombination. This new insight into the dynamical evolution of radiation defects points to a thermodynamic criterion for designing radiation-tolerant materials.

1. Introduction

The main technical impediment to the development of advanced nuclear power systems lies in the creation of radiation-resistant structural materials. Various approaches are under active research, ranging from oxide dispersion strengthened (ODS) steels [1], to nanograined alloys [2], to severely plastically deformed (SPD) materials [3]. Recently, a new class of materials, called single-phase concentrated solid solution alloys (SP-CSAs) [4], including high entropy alloys (HEAs) [5], has received great attention due to their potential radiation resistance [6]. SP-CSAs are typically composed of two or more principle elements in a simple, single-phase solid solution, with nearly equiatomic concentrations. The random arrangement of atoms results in a complex local atomic environment [7], with implications ranging from high strength [8] while retaining ductility [9], to high fracture toughness [10], to excellent corrosion resistance [11]. Moreover, recent experiments and simulations indicate that these single-phase alloys have significantly better radiation resistance than their corresponding elementary metals [6,12].

Varying alloy elemental concentrations and types changes the local atomic environment, which can significantly influence the migration energy barriers and pathways of radiation defects. This has been demonstrated by tuning the composition of alloys to increase their radiation damage tolerance. Wang et al. found that radiation-induced defect sizes resulting from ion irradiation of Ni-Cu alloys decrease when increasing the Cu concentration from 10% to 50% [13]. Jin et al. and Zhang et al. observed enhanced radiation tolerance in Ni-Fe alloys by increasing the Fe concentration up to 60% [14,15], and suggested chemical disorder to be a key factor for controlling radiation performance [14]. Molecular dynamics (MD) simulations of radiation damage accumulation have been studied intensively from elementary metals to many SP-CSAs [6,12,16], revealing that more alloying (both in species and concentrations) demonstrates higher radiation resistance. However, these investigations focus on the reduction of damage in a few selected alloys in comparison to elemental Ni. A comprehensive understanding of the effects of alloy composition, defect dynamics, damage accumulation, and defect recombination are necessary to gain a more fundamental basis for designing radiation tolerant alloys.

In this work, we study ion radiation-induced defect evolution and damage accumulation in elemental Ni and $Ni_{1-x}Fe_x$ alloys with x ranging from 10 to 90%. The face-centered cubic (FCC) structure is

* Corresponding author.
E-mail address: pcao@mit.edu (P. Cao).

https://doi.org/10.1016/j.actamat.2017.12.064
1359-6454/

considered so as to study the pure effect of the single variable of Fe concentration x on radiation resistance, without introducing any additional complexity of crystal structure. However, it should be noted that when x is larger than $\sim$ 70%, the FCC system is in a thermodynamically metastable state. We employ a hybrid Monte Carlo and Molecular Dynamics (MC+MD) approach (see the Methods section) to prepare well-mixed systems. MD is then utilized to impose consecutive radiation collision cascades to achieve radiation doses of about 0.5 DPA (displacements per atom) (See Methods). By analyzing defect production and evolution, we find that defect accumulation clearly shows a dependence on alloy composition, and the rate of damage accumulation is controlled by the speed of large defect cluster growth. The largest reduction in damage is observed near the minimum of mixing energy (see Fig. 2(c)), which we suggest as a parameter in governing radiation resistance. To obtain a more fundamental understanding of the results, we examined defect migration energy barriers and pathways of point defects in these alloys using the nudged elastic band (NEB) method [17]. The variance of these barriers, which reflects the complexity of the local potential energy landscape (PEL), indicates increasingly heterogeneous point defect migration in the more highly radiation-tolerant compositions. Our results provide atomistic details of damage evolution and reduction, suggesting a quantitative basis for developing radiation-tolerant materials.

2. Methods

2.1. Hybrid MC+MD simulations and atom swapping

One possible concern in atomistically simulating SP-CSAs involves the creation of the initial atomic structure. The approach used in previous MD studies [12,18,19] was to randomly replace one atom type with the other, which may not recreate truly mixed SP-CSA structures. This random procedure can produce local atomic structures with high potential energy, which are thermodynamically unstable. The as-prepared metastable system becomes a particular concern when simulating radiation damage, as the dissipation of radiation damage energy and structural relaxation of the initial high-energy atomic configuration would become convolved. Recently, an effort to construct SP-CSAs via a quasirandom structure was made in Ref. [20], where the Warren-Cowley short range order [21] was optimized to produce a truly random atomic structure. In this work, we use a hybrid MC+MD algorithm to prepare stable alloy systems. $Ni_{1-x}Fe_x$ alloys are modeled using the embedded atom method (EAM) potential developed by Bonny et al. [22]. This potential is an improved version of the Bonny 2011 potential [23], which was developed to model the production and evolution of collision cascade-induced defects. It has been extensively applied to successfully predict concentration-dependent radiation defects in NiFe alloys as observed in experiments [6,15]. We prepare the initial FCC alloy structures by randomly mixing Ni and Fe atoms at each specified composition. The simulation cell contains 108,000 atoms, and periodic boundary conditions are applied in all three directions in all simulations. A hybrid MC+MD algorithm [24,25] is used to anneal each generated system. In each MC trial step, a randomly selected Ni atom is swapped with another randomly selected Fe atom. The trial move is accepted with a probability of unity or $P = exp(-\Delta U/k_B T)$, whichever is smaller, depending on the value of ΔU, where ΔU is the change in system potential energy after the atom exchange and T is the chosen system temperature of 300 K. Following 100 MC trials, we perform 0.1 ps of MD simulation in the isothermal-isobaric condition (NPT ensemble). We repeat the above MC+MD procedures to anneal each alloy, and a total of 50,000 MC trials and 50 ps MD runs are performed. The equilibrated systems show much lower potential energies than those which were randomly generated (see Supplementary Fig. S1).

2.2. Molecular dynamics simulations

The MD method as implemented in LAMMPS [26] is utilized to simulate self-ion radiation damage in each annealed system. To deal with high energy radiation damage collisions, a Ziegler-Biersack-Littmark (ZBL) repulsive potential [27,28] is smoothly joined to the aforementioned EAM potentials [29], and an adaptive time step algorithm is used to limit atomic movement to 0.05 Å in each timestep. The choice of ZBL joining parameters could affect the generation of primary damage as discussed by Stoller et al. [30]. In this work, the smoothly joined potentials adequately capture the features of Fe concentration-dependent radiation defect production and evolution as seen in ion irradiation experiments. We first relax each system at 300 K for 100 ps. An atom is randomly chosen as the primary knock-on atom (PKA), and we shift the entire cell to move the PKA to the center. This avoids the damage cascade from reaching the system boundaries. The PKA is assigned a kinetic energy of 5 keV, and 50,000 adaptive timesteps of MD simulation ($\sim$45 ps) are performed. The Nosé-Hoover temperature-rescaling thermostat [31,32] is applied to the atoms at the sides of the simulation cell with a width of half the lattice constant, to absorb the collision cascade energy and cool the system to 300 K. This process is repeated with each PKA randomly chosen and shifted to the center of the cell, simulating the spatially random arrival of radiation damage cascades. Up to 1500 consecutive 5 keV cascades result in radiation damage levels of $\sim$0.5 DPA. The short simulation time (an inherent limitation of MD) between collision cascades yields a dose rate several orders of magnitude higher than that in experimental conditions. Although the difference in dose rate between MD and experiments is quite large, a recent study using similar approaches has shown good agreement with experiments [6]. We performed twelve independent 1500 consecutive 5 keV cascade simulation runs for each system to obtain more reliable results. Defects are identified by comparing the irradiated system with the initial perfect structure using Wigner-Seitz cell method. The defects analysis and visualization are performed with OVITO package [33] with an adaptive common neighbor analysis.

2.3. Defect migration energy barrier calculations

We compute vacancy and interstitial migration energy barriers with the climbing image nudged elastic band (NEB) method [17]. We start with the MC+MD equilibrated system. By removing one atom, we create a vacancy and consider all twelve (not necessarily equivalent) diffusion pathways on the FCC lattice by exchanging with the twelve first nearest neighbors. With the NEB method, we find the saddle point along each minimum energy pathway, and from that the migration energy barrier is calculated (see Supplemental Information). We consider all possible vacancy sites in the relaxed system, and the energy barriers corresponding to $\sim$10,368 pathways are evaluated. Similarly, we insert Ni or Fe atoms to create [100] dumbbell interstitials. Note that due to local lattice distortion, placing an atom at the designated position may not create the desired dumbbell structure after relaxation. Therefore we take extreme care to confirm the initial and final configurations for interstitial migration. Only valid rotations are considered in our calculations.

3. Results

3.1. Annealed alloy systems and their mixing energies

We take extra care to prepare a stable, well-equilibrated single-phase alloy using the hybrid MC+MD method. We found that

across all alloys studied, the MC+MD swaps effectively lower system energy, indicating a more energetically favorable system (See Supplementary Fig. S1). To compare the atomic structural differences between the two systems (randomly prepared and MC+MD annealed), we show changes in the radial distribution function $g(r)$ of Ni and Fe in $Ni_{40}Fe_{60}$ in Fig. 1(a). Both the Ni and Fe distributions exhibit a smaller first peak and a larger third peak in $g(r)$ in the annealed system, showing that more dissimilar atoms become first nearest neighbors after the MC+MD swaps. This change in $g(r)$ implies that a better mixed Ni-Fe structure is obtained after the annealing operation.

The equilibrated Ni-Fe alloy systems enable precise measurement of the mixing energy ΔE, a change in energy caused by elemental mixing. Before Ni and Fe mixing, the system energy E_0 can be computed as $E_0 = E_{Ni}N_{Ni} + E_{Fe}N_{Fe}$, where E_{Ni}, E_{Fe} are per-atom energies of Ni and Fe, and N_{Ni}, N_{Fe} are the numbers of Ni and Fe atoms, respectively. We compute the mixed system energy E_f from the MC+MD equilibrated system. In the inset of Fig. 1(b), we show how E_0 and E_f vary with changing Fe concentration. The mixing energy ΔE defined as $\Delta E = E_f - E_0$ is plotted as a function of Fe concentration in Fig. 1(b), where a local minimum is noted near the vicinity of equiatomic concentration.

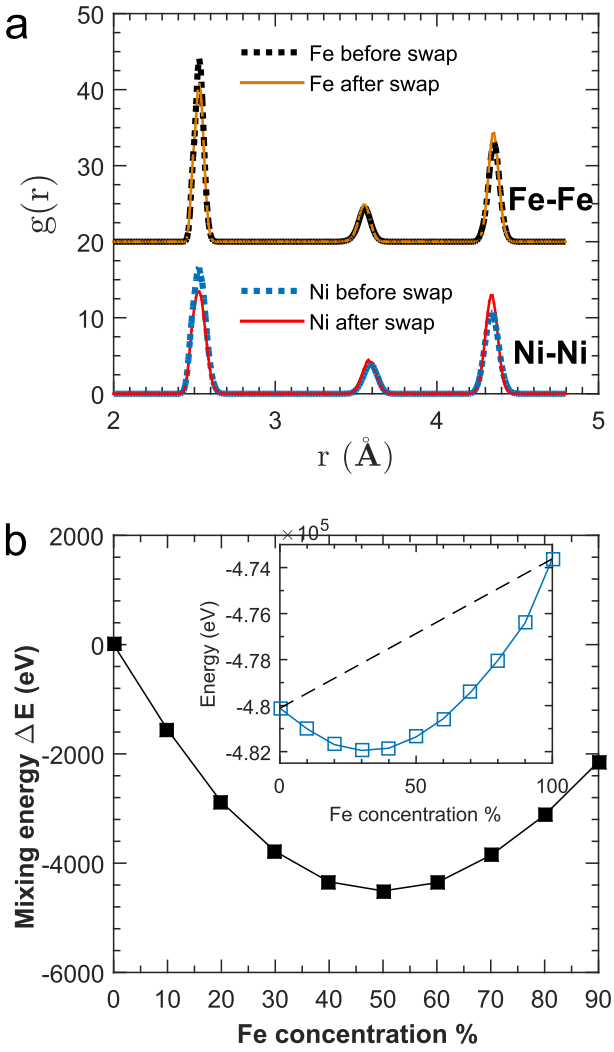

Fig. 1. (a) Radial distribution function $g(r)$ for Fe-Fe and Ni-Ni before (i.e. randomly generated configuration) and after MC+MD swap annealing of $Ni_{40}Fe_{60}$. (b) Mixing energy ΔE versus Fe concentration. The blue squares in the inset show the energy of the annealed system E_f, while the black dashed line shows the energy E_0 before mixing. (For interpretation of the references to color in this figure legend, the reader is referred to the Web version of this article.)

3.2. Radiation damage accumulation

The level of defect production during irradiation can be obtained by analyzing the atomic structures from the MD simulations of consecutive damage cascades. In Fig. 2(a), we present a heat map of damage accumulation, with the x- and y-axes representing Fe concentration and number of cascades, respectively. The map is color coded by the number of defects (Frenkel pairs) remaining after each damage cascade. The map shows that the level of damage increases with subsequent cascades, while the rate of defect accumulation clearly depends on alloy composition. Fig. 2(b) provides a supplementary view on the trend for selected compositions with Fe ranging from 0% to 50%. It can be seen that the number of defects produced is essentially the same for these compositions up to ~50 cascades, implying that defect production from the initial stages of radiation damage depends weakly on composition. At this stage, damage from consecutive cascades has not yet begun to significantly overlap, and the discrete cascades mainly produce localized point defects (see Fig. 4(a) and (c)). However, the curves start to separate after 100 cascades, and defect accumulation shows a clear dependence on composition with a significant reduction in damage with increasing Fe. It is reasonable to assume that this observed damage reduction at high Fe concentrations is the result of enhanced of defect recombination.

To clearly see how damage accumulation depends on material composition, we show in Fig. 2(c) the number of defects as a function of Fe concentration at different damage levels. At all damage levels, the number of defects initially decreases with increasing Fe, and then starts to increase. The very low damage level of 300 cascades displays a maximum damage reduction near the equiatomic composition, i.e. 50% Fe, at which the system also has the largest magnitude of mixing energy as shown in Fig. 1(b). This indicates a close relationship between damage reduction and mixing energy. With an increasing number of collision cascades, it can be seen that the composition with the minimum number of defects slightly shifts to 60% Fe, in agreement with recent ion irradiation experiments of the irradiation of Ni-Fe alloys [14,15], in which $Ni_{40}Fe_{60}$ was found to be the most damage tolerant. The interesting shift of minimum defects at higher damage levels implies the effects of defect dynamics and diffusion on damage reduction, which will be analyzed in detail in the following section. For the verification of simulations, we compare the simulated Fe concentration-dependent damage with a recent experiment [15] in Fig. 2(c). The inset shows the defect level as experimentally measured by backscattering yield for various Fe concentrations up to 60%. It can be seen that the defect accumulation slows down with increasing Fe concentration, which is consistent with the current simulation.

We further connect the amount of radiation damage with the mixing energy ΔE in Fig. 2(d), where the number of surviving defects is plotted against mixing energy for all simulated materials (including Ni and nine $Ni_{1-x}Fe_x$ alloys). In the early stages of radiation damage (300 cascades), the damage is strongly correlated with mixing energy ΔE with an excellent linear fit. After 900 cascades, the damage is still an essentially linear function of ΔE, though it does exhibit a somewhat weaker dependence. The results show that the energy change during alloy mixing correlates well with radiation tolerance, suggesting that ΔE can serve as a key metric when designing radiation-resistant single-phase alloys.

3.3. Atomistic processes of defect evolution

Fig. 2 summarized the defects produced by radiation for

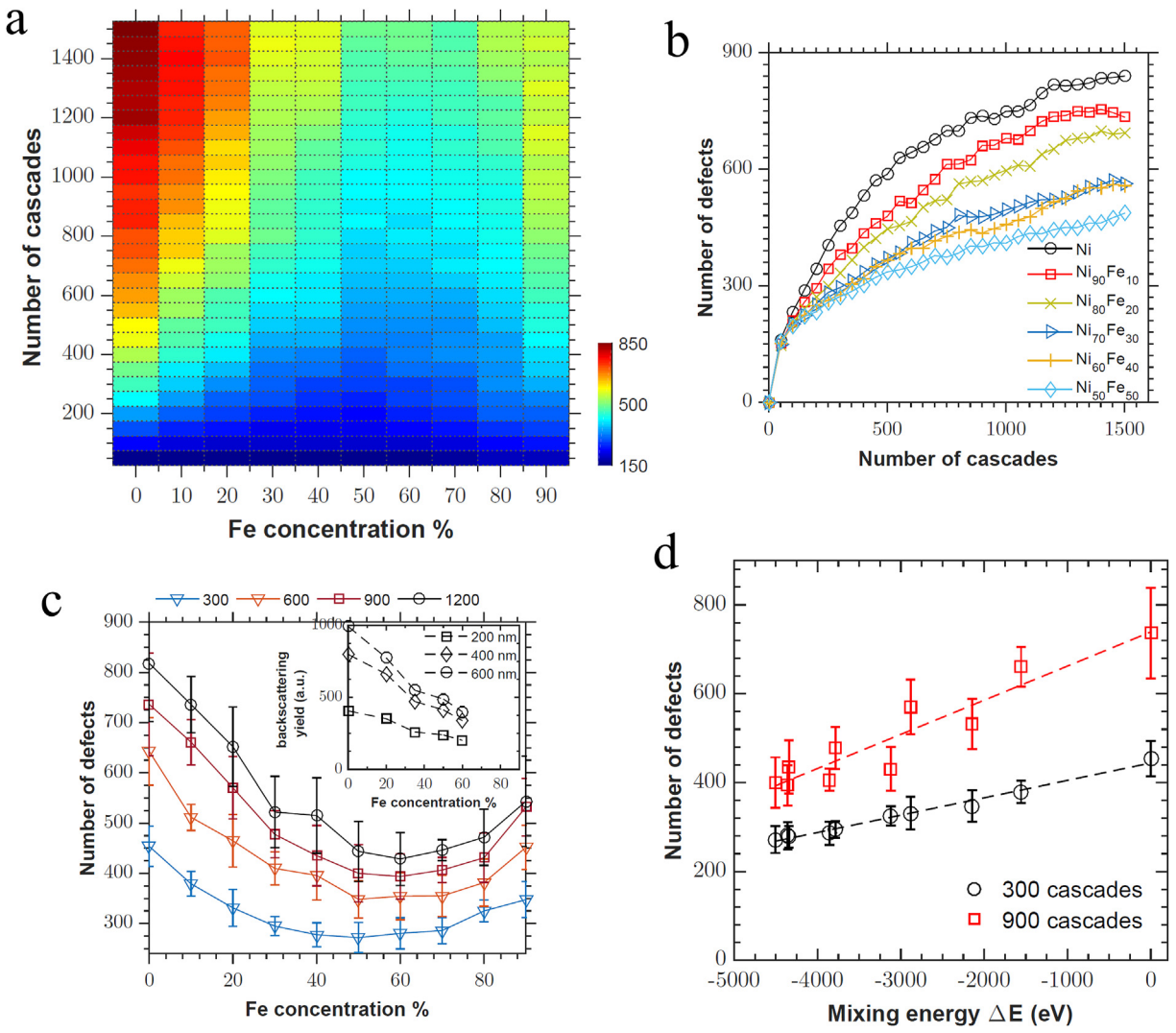

Fig. 2. (a) Damage production map for elemental Ni and $Ni_{1-x}Fe_x$ alloys with various Fe concentrations, subjected to radiation damage up to 1500 consecutive cascades (~ 0.5 DPA). For each composition, the map is color coded by the average number of defects (Frenkel pairs) produced from twelve independent simulations. (b) Number of defects as a function of number of cascades for Ni and various Ni-Fe alloys as indicated. (c) Fe concentration-dependent defect production at different stages of radiation damage (300, 600, 900 and 1200 cascades). The error bars indicate one standard deviation. The inset shows experimentally measured radiation damage at different depths, as a function of Fe concentration from 0 to 60%. The data are adapted from Ref. [15]. (d) Linear correlation between radiation damage and mixing energy ΔE for Ni and nine $Ni_{1-x}Fe_x$ alloys. (For interpretation of the references to color in this figure legend, the reader is referred to the Web version of this article.)

different $Ni_{1-x}Fe_x$ compositions, indicating that stoichiometry has a significant effect on damage reduction. One then must know the details of defect evolution associated with the observed damage accumulation, to mechanistically understand the dynamical processes of radiation damage. A detailed analysis of defect size distributions as a function of cascade in Ni and $Ni_{40}Fe_{60}$ is presented in Fig. 3(a–b). The size distributions (bar graphs) are colored by the number of defects in each size bin, ranging from 1 to 1000 atoms. These plots show the evolution of small (size < 50) and large (size > 80) defects to clearly differ. The number of small defects quickly saturates for both materials (Fig. 3(c)), while larger defects continue growing through the simulated damage stages (Fig. 3(d)). Recall in Fig. 2(b) that the total number of defects continues to increase with successive cascades. It is reasonable to conclude from Fig. 3 that the radiation damage accumulation observed in Fig. 2 (i.e. total defect production) is essentially governed by the growth of larger clusters. The behaviours of radiation-induced defects are particularly interesting when comparing $Ni_{40}Fe_{60}$ with Ni, as one can see in $Ni_{40}Fe_{60}$ that the saturation density of small defects is lower, and the growth of large clusters is significantly slower.

To see which defect types could be associated with the behavior in Fig. 3, we turn to the details of the atomic structures of the damaged materials. The spatial distributions of defect structures in Ni and $Ni_{40}Fe_{60}$ after different numbers of cascades are presented in Fig. 4. After 50 cascades, both Ni and its alloys display similar point defect distributions (Fig. 4(a) and (d)). However, after 500 cascades, one can clearly see the growth in defect cluster size, and ordered defect structures such as stacking faults and dislocation loops are formed as shown in Fig. 4(b) and (e). The formation of ordered defects and their growth is more pronounced in Ni (Fig. 4(c)), as far more atoms are involved in processes of defect agglomeration in Ni compared to $Ni_{40}Fe_{60}$ (Fig. 4(f)). The clear details of defect growth and interaction are illustrated in the supplementary movies. One can see stable defect structures forming at the early stages of radiation damage (about 100 cascades) in Ni, which rapidly expand in size when interacting with surrounding defects. By contrast $Ni_{40}Fe_{60}$ develops stable

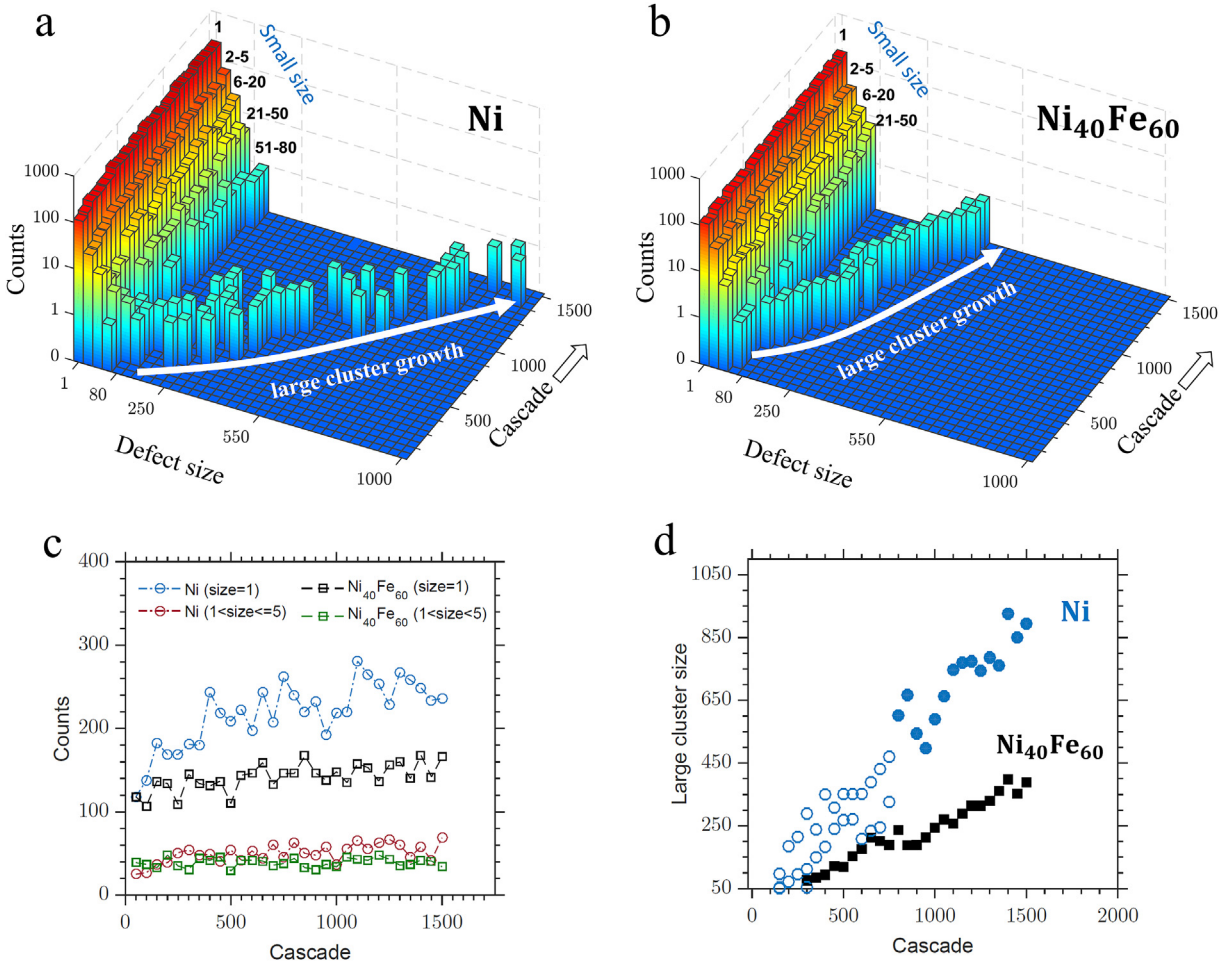

Fig. 3. Evolution of defect size as a function of damage cascades for (a) Ni and (b) $Ni_{40}Fe_{60}$. (c) Number of small defects (1–5 atoms) versus cascade number. (d) Comparison of the growth of large clusters in Ni and $Ni_{40}Fe_{60}$. The filled circles and squares denotes the existence of only one large cluster, while the open circles mean two or more large clusters are present.

defect structures after ~380 cascades, which implies inherent resistance to defect growth.

Supplementary video related to this article can be found at https://doi.org/10.1016/j.actamat.2017.12.064.

The results presented in Figs. 3–4 show that certain alloy compositions have higher resistances to the formation of large clusters. This may be interpreted from the two perspectives of thermodynamic mixing energy and defect dynamics. At the system level, the large absolute value of mixing energy of an alloy implies a strong propensity for better mixing between Ni and Fe atoms, and an inherently energetic resistance to the formation of large-scale defect structures. This point has been discussed before, as Zhang et al. have noted energy dissipation as a controlling factor in radiation resistance [14]. This is because most defects represent less elemental mixing with higher potential energy when compared to a properly mixed, unirradiated alloy. At the microscale, the dynamic behaviors of defects play an essential role in damage reduction and accumulation. In Fig. 2(b–c), the increase in radiation damage resistance when increasing the Fe concentration from 0 to 60% is attributed to the enhancement of defect recombination and annihilation. This deduction is also supported by the defect evolution movies in the Supplemental Information. To understand the defect kinetics, we study the dynamical diffusion of vacancies and interstitials by examining their migration pathways and energetic barriers.

3.4. Heterogeneity of defect migration

The dynamical behavior of defects in a material can be determined by its underlying PEL, where defect migration corresponds to the hopping (thermal activation) process between neighboring local energy minima. A schematic illustration of hopping in the PEL is shown in Fig. 5(a–b). The types of migration pathways of point defects in Ni are very limited due to the inherent symmetry in the PEL. In contrast to Ni, the migration pathways are much more complex in alloys as a result of local atomic complexity and lattice distortion, which generate anisotropic stress fields and make diffusion intrinsically heterogeneous (Fig. 5(b)). Here, we explore the characteristics of PELs by sampling energy barriers $E_\mathbf{b}$ along defect (interstitial and vacancy) migration pathways, where $E_\mathbf{b}$ is the energy difference between an initial local minimum and a nearby saddle point. We sampled a significantly large number of pathways to obtain good statistics (see Methods). The histograms in Fig. 5(c) display energy barrier distributions for vacancy diffusion in three $Ni_{1-x}Fe_x$ alloys. Pure Ni has a constant vacancy migration energy of 1.09 eV indicated by the black dashed line (Fig. S4 and S5 of Supplementary Information for all compositions). The variance of these energy barrier distributions reflects the roughness of the PEL, and hence the heterogeneity of diffusion.

The histograms in Fig. 5(c) show considerable spread in the

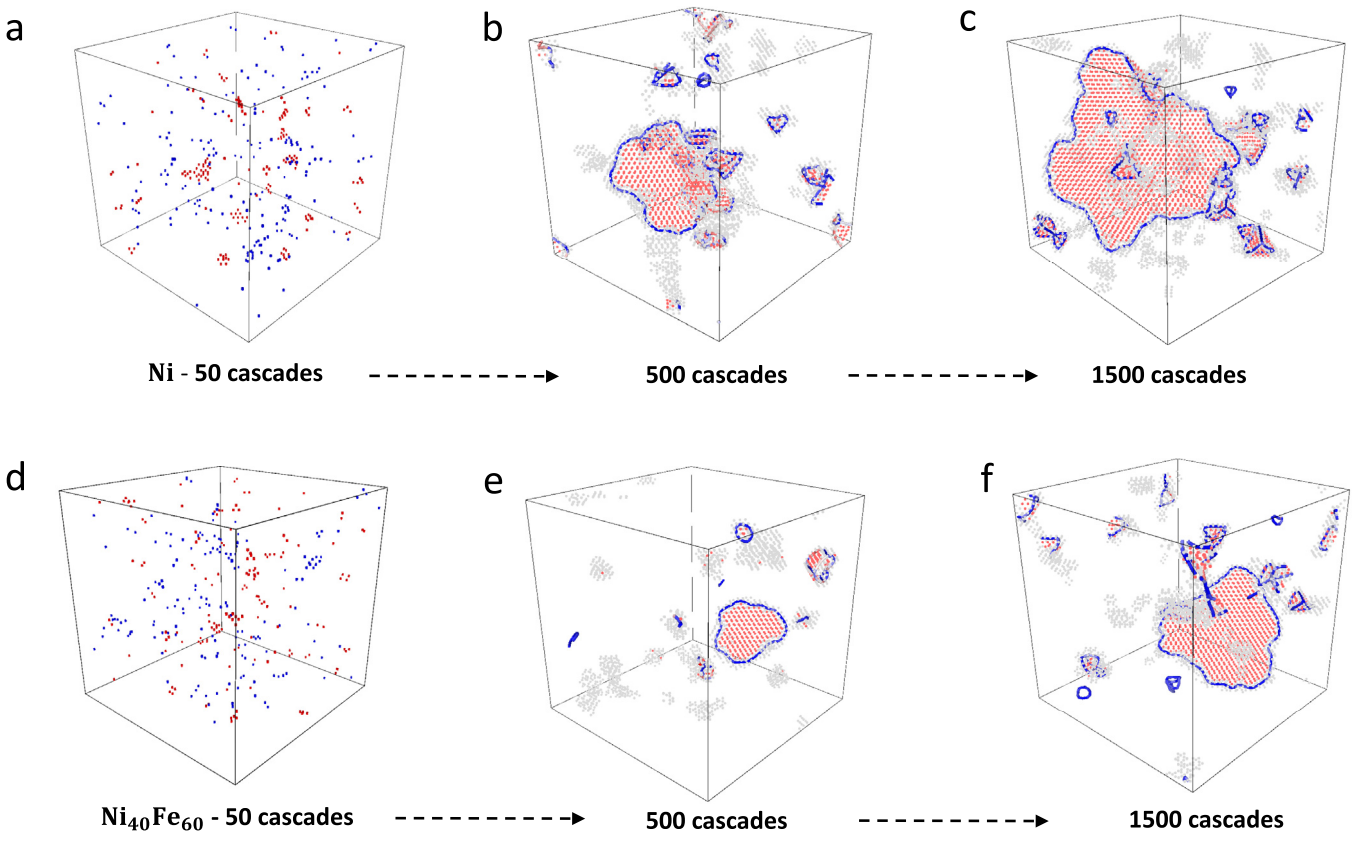

Fig. 4. Defect distributions at different damage stages in Ni and $Ni_{40}Fe_{60}$. (a), (d) Point defects produced after 50 cascades. Red indicates interstitials, while blue shows vacancies. (b), (c) and (e), (f) Ordered defect structures formed at 500 cascades and grown in size at 1500 cascades in Ni and $Ni_{40}Fe_{60}$, respectively. Only large defect cluster (non-fcc structure) are shown. The red atoms are hexagonally close packed (hcp) stacking faults, while the solid lines indicate dislocations. (For interpretation of the references to color in this figure legend, the reader is referred to the Web version of this article.)

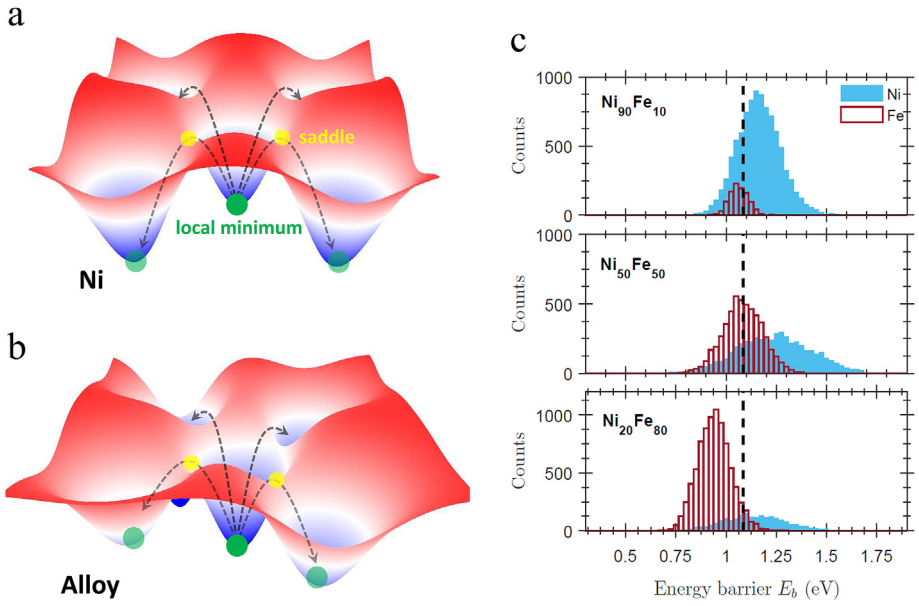

Fig. 5. (a–b) Schematic illustrations of defect migration pathways in the potential energy landscape (PEL) for Ni (a) and (b) Ni-Fe alloy, respectively. The energy difference between a local minimum and nearby saddle point constitutes the energy barrier for defect migration. (c) Distributions of Ni- and Fe-vacancy migration energy barriers in $Ni_{90}Fe_{10}$, $Ni_{50}Fe_{50}$, and $Ni_{20}Fe_{80}$. The black dashed line shows the vacancy migration barrier in elemental Ni.

distribution of local defect migration barriers. While the mean value of each distribution would be cited as its 'migration energy,' the broad spread in local migration energies should be noted especially for compositions near $Ni_{40}Fe_{60}$. Similar computations

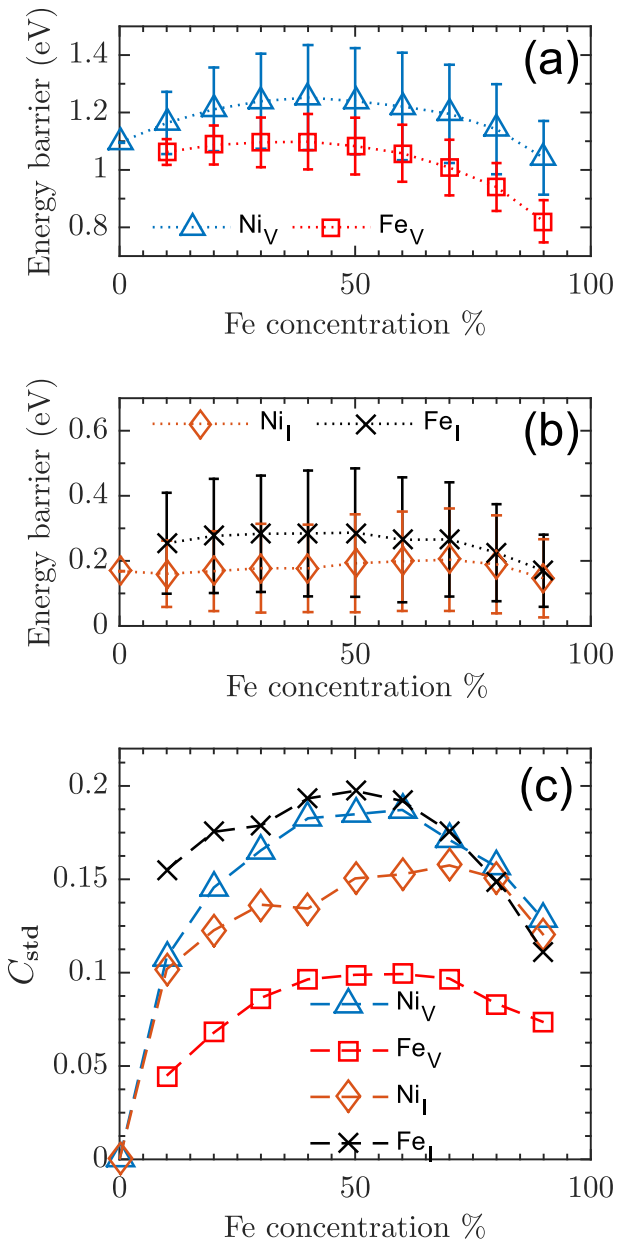

Fig. 6. (a) Average vacancy migration energy barrier versus Fe concentration in $Ni_{1-x}Fe_x$ alloys. The error bars represent one standard deviation c_{std}. (b) Average interstitial migration energy barrier versus Fe concentration. (c) Standard deviation of the migration energy barrier c_{std} for all defect types versus Fe concentration.

for the full range of $Ni_{1-x}Fe_x$ alloys are summarized in Fig. 6(a–b). The diffusion processes are dominated by low energy pathways [34] according to transition state theory [35], which means that unlike elementary Ni, diffusion in $Ni_{1-x}Fe_x$ alloys is spatially heterogeneous and directionally anisotropic. We calculate the standard deviation c_{std} of energy barriers in each alloy to quantify its diffusional heterogeneity, as shown in Fig. 6(c). The values of c_{std} for both vacancies and interstitials increase with Fe concentration, and then decrease at around 60% Fe. Particularly interesting is the observation that c_{std} negatively correlates with the accumulation of radiation damage (Fig. 2(c)). The comparison suggests that the more complex PEL of alloys results in heterogeneous diffusion of vacancies and interstitials, enhancing the recombination of defects.

4. Discussion

By simulating consecutive damage cascades in Ni and Ni-Fe alloys, we show that defect production in the initial stages of radiation damage is similar across all $Ni_{1-x}Fe_x$ alloys. Nevertheless, some alloys are more efficient at annihilating defects and restoring their crystal structures over longer periods of irradiation, thus demonstrating better radiation tolerance. We found that the such tolerance correlates strongly with mixing energy ΔE, thus minimizing ΔE may be an indicator of improved irradiation performance.

The notion that the energy of mixing (related directly to alloying energy or the enthalpy of formation) may be a descriptor of stability in catalysts has been discussed previously by Greely et al. [36] and Vej-Hansen et al. [37], who demonstrated a strong correlation between diffusion barriers of the minority component and alloying energy in Pt/Pd/Al-based binary alloys. Mantina et al. show that these energies are intimately related to the first-principles calculation of diffusion constants [38]. In the scenario of radiation damage in Ni-Fe alloys, we have shown that such a simple thermodynamic measure scales extremely well with the resistance to disorder.

A mechanistic explanation for the enhanced radiation resistance of alloys which energetically favor mixing lies in the modification of defect migration dynamics. The different compositions and atomic sizes of elements in SP-CSAs substantially reduce electron, phonon, and magnon mean free paths [14], which influence defect formation energies and their dynamical evolution. The differences of atomic size and type specifically lead to lattice distortion, producing local structural complexity. It is known that the defect diffusion pathways and their associated migration barriers are governed by their surrounding atomic structures. The wide distribution of migration barriers on the complex PEL results in significant heterogeneous defect diffusion processes, which enhance the recombination of radiation-induced defects as observed in our simulations. It has been reported in recent experiments that the heterogeneity of defect diffusion makes alloys more radiation resistant than pure metals. Lu et al. [39] explained in a recent study that the three dimensional (3D) migration of interstitial clusters rather than one dimensional (1D) crowdion diffusion accounts for the enhanced radiation resistance of NiFe, NiCoFe, NiCoFeCr, and NiCoFeCrMn. The basic understanding is that defects moving in 3D forms, instead of faster-moving 1D crowdions, are confined to smaller regions of material and therefore increase the likelihood of recombination over clustering by long range migration. Here, we consider diffusional heterogeneity from the spectrum of migration barriers of point defects. It has been found that interstitial diffusion in highly radiation resistant alloys is significantly heterogeneous (high standard deviation in the distribution of migration barriers), which could potentially slow the clustering movement of interstitials across complex PELs. Hence a higher defect recombination rate is expected, which eventually results in fewer residual defects in the system.

To summarize, our simulation results on Ni-Fe alloys show that there is a strong correlation between the energy of mixing and radiation resistance. Conceptually, defect clustering becomes energetically unfavorable in SP-CSAs that strongly prefer mixing, and an enhanced defect recombination is then expected. The general understanding is that local compositional complexity significantly adjusts defect migration behavior, and ultimately modifies radiation performance. From a quantitative point of view, the computation of point defect diffusion barriers demonstrated increasing heterogeneity of defect mobility in more radiation-resistant alloys. Further study is needed to confirm whether SP-CSAs containing more elements exhibit the same properties, and

whether the energy of mixing correlates well with radiation resistance in more complex alloy systems. In the end, minimizing the mixing energy and enhancing diffusional heterogeneity in SP-CSAs may represent a promising design criterion to develop improved radiation-resistant materials for nuclear applications.

Data linking

All data files which support the findings of this study are available on our public data repository [40].

Acknowledgements

We thank Ju Li and Sidney Yip at MIT for helpful discussions. **Funding:** This work was supported by the Electric Power Research Institute (EPRI) under Contract No. MA-10002739, and by the Idaho National Laboratory (INL) Nuclear University Consortium (NUC) under the Laboratory Directed Research and Development (LDRD) Grant No. 10-112583. **Author contributions:** P.H.C. and M.P.S. designed the project. P.H.C. implemented the simulation model. M.M.J. and P.H.C. conducted the simulations. M.M.J., P.H.C. and M.P.S. analyzed the data and wrote the paper.

Appendix A. Supplementary data

Supplementary data (figures and movies) related to this article can be found at https://doi.org/10.1016/j.actamat.2017.12.064.

References

[1] J. Brodrick, D. Hepburn, G. Ackland, Mechanism for radiation damage resistance in yttrium oxide dispersion strengthened steels, J. Nucl. Mater. 445 (1) (2014) 291–297.
[2] C. Sun, S. Zheng, C.C. Wei, Y. Wu, L. Shao, Y. Yang, K.T. Hartwig, S.A. Maloy, S.J. Zinkle, T.R. Allen, H. Wang, X. Zhang, Superior radiation-resistant nano-engineered austenitic 304L stainless steel for applications in extreme radiation environments, Sci. Rep. 5 (2015) 7801.
[3] I. Beyerlein, A. Caro, M. Demkowicz, N. Mara, A. Misra, B. Uberuaga, Radiation damage tolerant nanomaterials, Mater. Today 16 (11) (2013) 443–449.
[4] B. Cantor, I. Chang, P. Knight, A. Vincent, Microstructural development in equiatomic multicomponent alloys, Mater. Sci. Eng. A 375 (2004) 213–218.
[5] Y. Zhang, T.T. Zuo, Z. Tang, M.C. Gao, K.A. Dahmen, P.K. Liaw, Z.P. Lu, Microstructures and properties of high-entropy alloys, Prog. Mater. Sci. 61 (2014) 1–93.
[6] F. Granberg, K. Nordlund, M.W. Ullah, K. Jin, C. Lu, H. Bei, L. Wang, F. Djurabekova, W. Weber, Y. Zhang, Mechanism of radiation damage reduction in equiatomic multicomponent single phase alloys, Phys. Rev. Lett. 116 (13) (2016), 135504.
[7] Y. Zhang, K. Jin, H. Xue, C. Lu, R.J. Olsen, L.K. Beland, M.W. Ullah, S. Zhao, H. Bei, D.S. Aidhy, et al., Influence of chemical disorder on energy dissipation and defect evolution in advanced alloys, J. Mater. Res. 31 (16) (2016) 2363–2375.
[8] J.-W. Yeh, S.-K. Chen, S.-J. Lin, J.-Y. Gan, T.-S. Chin, T.-T. Shun, C.-H. Tsau, S.-Y. Chang, Nanostructured high-entropy alloys with multiple principal elements: novel alloy design concepts and outcomes, Adv. Eng. Mater. 6 (5) (2004) 299–303.
[9] G. Salishchev, M. Tikhonovsky, D. Shaysultanov, N. Stepanov, A. Kuznetsov, I. Kolodiy, A. Tortika, O. Senkov, Effect of Mn and V on structure and mechanical properties of high-entropy alloys based on CoCrFeNi system, J. Alloys Compd. 591 (2014) 11–21.
[10] H. Zhang, Y. He, Y. Pan, Enhanced hardness and fracture toughness of the laser-solidified FeCoNiCrCuTiMoAlSiB$_{0.5}$ high-entropy alloy by martensite strengthening, Scr. Mater. 69 (4) (2013) 342–345.
[11] Y. Qiu, M.A. Gibson, H.L. Fraser, N. Birbilis, Corrosion characteristics of high entropy alloys, Mater. Sci. Technol. 31 (10) (2015) 1235–1243.
[12] M.W. Ullah, D.S. Aidhy, Y. Zhang, W.J. Weber, Damage accumulation in ion-irradiated Ni-based concentrated solid-solution alloys, Acta Mater. 109 (2016) 17–22.
[13] L. Wang, S. Zinkle, R. Dodd, G. Kulcinski, Effects of preinjected helium in heavy-ion irradiated nickel and nickel-copper alloys, Metal. Trans. A 21 (7) (1990) 1847–1851.
[14] Y. Zhang, G.M. Stocks, K. Jin, C. Lu, H. Bei, B.C. Sales, L. Wang, L.K. Béland, R.E. Stoller, G.D. Samolyuk, et al., Influence of chemical disorder on energy dissipation and defect evolution in concentrated solid solution alloys, Nat. Commun. 6 (2015) 8736.
[15] K. Jin, W. Guo, C. Lu, M.W. Ullah, Y. Zhang, W.J. Weber, L. Wang, J.D. Poplawsky, H. Bei, Effects of Fe concentration on the ion-irradiation induced defect evolution and hardening in Ni-Fe solid solution alloys, Acta Mater. 121 (2016) 365–373.
[16] M.W. Ullah, H. Xue, G. Velisa, K. Jin, H. Bei, W.J. Weber, Y. Zhang, Effects of chemical alternation on damage accumulation in concentrated solid-solution alloys, Sci. Rep. 7 (2017) 4146.
[17] G. Henkelman, B.P. Uberuaga, H. Jónsson, A climbing image nudged elastic band method for finding saddle points and minimum energy paths, J. Chem. Phys. 113 (22) (2000) 9901–9904.
[18] G. Velişa, M.W. Ullah, H. Xue, K. Jin, M.L. Crespillo, H. Bei, W.J. Weber, Y. Zhang, Irradiation-induced damage evolution in concentrated Ni-based alloys, Acta Mater. 135 (2017) 54–60.
[19] S. Rao, C. Varvenne, C. Woodward, T. Parthasarathy, D. Miracle, O. Senkov, W. Curtin, Atomistic simulations of dislocations in a model bcc multicomponent concentrated solid solution alloy, Acta Mater. 125 (2017) 311–320.
[20] S. Zhao, G.M. Stocks, Y. Zhang, Defect energetics of concentrated solid-solution alloys from ab initio calculations: Ni$_{0.5}$Co$_{0.5}$, Ni$_{0.5}$Fe$_{0.5}$, Ni$_{0.8}$Fe$_{0.2}$ and Ni$_{0.8}$Cr$_{0.2}$, Phys. Chem. Chem. Phys. 18 (34) (2016) 24043–24056.
[21] J. Cowley, An approximate theory of order in alloys, Phys. Rev. 77 (5) (1950) 669.
[22] G. Bonny, N. Castin, D. Terentyev, Interatomic potential for studying ageing under irradiation in stainless steels: the FeNiCr model alloy, Model. Simulat. Mater. Sci. Eng. 21 (8) (2013), 085004.
[23] G. Bonny, D. Terentyev, R. Pasianot, S. Poncé, A. Bakaev, Interatomic potential to study plasticity in stainless steels: the FeNiCr model alloy, Model. Simulat. Mater. Sci. Eng. 19 (8) (2011), 085008.
[24] H.B. Lee, F.B. Prinz, W. Cai, Atomistic simulations of surface segregation of defects in solid oxide electrolytes, Acta Mater. 58 (6) (2010) 2197–2206.
[25] B. Sadigh, P. Erhart, A. Stukowski, A. Caro, E. Martinez, L. Zepeda-Ruiz, Scalable parallel Monte Carlo algorithm for atomistic simulations of precipitation in alloys, Phys. Rev. B 85 (18) (2012), 184203.
[26] S. Plimpton, Fast parallel algorithms for short-range molecular dynamics, J. Comput. Phys. 117 (1) (1995) 1–19.
[27] J.F. Ziegler, J.P. Biersack, U. Littmark, The Stopping and Range of Ions in Solids, Pergamon Press, 1985.
[28] K. Nordlund, M. Ghaly, R. Averback, M. Caturla, T.D. de La Rubia, J. Tarus, Defect production in collision cascades in elemental semiconductors and fcc metals, Phys. Rev. B 57 (13) (1998) 7556.
[29] X.-M. Bai, A.F. Voter, R.G. Hoagland, M. Nastasi, B.P. Uberuaga, Efficient annealing of radiation damage near grain boundaries via interstitial emission, Science 327 (5973) (2010) 1631–1634.
[30] L.K. Béland, C. Lu, Y.N. Osetskiy, G.D. Samolyuk, A. Caro, L. Wang, R.E. Stoller, Features of primary damage by high energy displacement cascades in concentrated ni-based alloys, J. Appl. Phys. 119 (8) (2016), 085901.
[31] S. Nosé, A molecular dynamics method for simulations in the canonical ensemble, Mol. Phys. 52 (2) (1984) 255–268.
[32] W.G. Hoover, Canonical dynamics: equilibrium phase-space distributions, Phys. Rev. A 31 (1985) 1695–1697.
[33] A. Stukowski, Structure identification methods for atomistic simulations of crystalline materials, Model. Simul. Mater. Sci. Eng. 20 (4) (2012), 045021.
[34] P. Cao, D. Wells, M.P. Short, Anisotropic ion diffusion in [small alpha]-cr2o3: an atomistic simulation study, Phys. Chem. Chem. Phys. 19 (2017) 13658–13663.
[35] K.J. Laidler, M.C. King, Development of transition-state theory, J. Phys. Chem. 87 (15) (1983) 2657–2664.
[36] J. Greeley, I.E.L. Stephens, A.S. Bondarenko, T.P. Johansson, H.A. Hansen, T.F. Jaramillo, J. Rossmeisl, I. Chorkendorff, J.K. Nørskov, Alloys of platinum and early transition metals as oxygen reduction electrocatalysts, Nat. Chem. 1 (2009) 552–556.
[37] U.G. Vej-Hansen, J. Rossmeisl, I.E.L. Stephens, J. Schiotz, Correlation between diffusion barriers and alloying energy in binary alloys, Phys. Chem. Chem. Phys. 18 (2016) 3302–3307.
[38] M. Mantina, Y. Wang, L. Chen, Z. Liu, C. Wolverton, First principles impurity diffusion coefficients, Acta Mater. 57 (14) (2009) 4102–4108.
[39] C. Lu, L. Niu, N. Chen, K. Jin, T. Yang, P. Xiu, Y. Zhang, F. Gao, H. Bei, S. Shi, et al., Enhancing radiation tolerance by controlling defect mobility and migration pathways in multicomponent single-phase alloys, Nat. Commun. 7 (2016), 13564.
[40] Data Repository for NiFe Radiation Resistance Manuscript, 2017, https://doi.org/10.5281/zenodo.886560 available at: http://www.github.com/shortlab/2017NiFe-Mixing/.